Monthly Notices of the ROYAL ASTRONOMICAL SOCIETY

MNRAS **510,** L18–L23 (2022) https://doi.org/10.1093/mnrasl/slab117
Advance Access publication 2021 October 27

The fast radio burst population evolves, consistent with the star formation rate

C. W. James [1]★ J. X. Prochaska,[2,3] J.-P. Macquart [1]† F. O. North-Hickey,[1] K. W. Bannister[4] and A. Dunning[4]

[1]*International Centre for Radio Astronomy Research, Curtin University, Bentley, WA 6102, Australia*
[2]*Kavli Institute for the Physics and Mathematics of the Universe, 5-1-5 Kashiwanoha, Kashiwa 277-8583, Japan*
[3]*Astronomy Department, University of Washington, Seattle, WA 98195, USA*
[4]*CSIRO Astronomy and Space Science, PO Box 76, Epping, NSW 1710, Australia*

Accepted 2021 October 19. Received 2021 October 19; in original form 2021 January 20

ABSTRACT

Fast radio bursts (FRBs) are extremely powerful sources of radio waves observed at cosmological distances. We use a sophisticated model of FRB observations – presented in detail in a companion paper – to fit FRB population parameters using large samples of FRBs detected by ASKAP and Parkes, including seven sources with confirmed host galaxies. Our fitted parameters demonstrate that the FRB population evolves with redshift in a manner consistent with, or faster than, the star formation rate (SFR), ruling out a non-evolving population at better than 98 per cent CL (depending on modelling uncertainties). Our estimated maximum FRB energy is $\log_{10} E_{\rm max}[{\rm erg}] = 41.70^{+0.53}_{-0.06}$ (68 per cent CL) assuming a 1 GHz emission bandwidth, with slope of the cumulative luminosity distribution $\gamma = -1.09^{+0.14}_{-0.10}$. We find a log-mean host DM contribution of 129^{+66}_{-48} pc cm^{-3} on top of a typical local (interstellar medium and halo) contribution of $\sim$80 pc cm^{-3}, which is higher than most literature values. These results are insensitive to assumptions of the FRB spectral index, and are consistent with the model of FRBs arising as the high-energy limit of magnetar bursts, but allow for FRB progenitors that evolve faster than the SFR.

Key words: methods: statistical – fast radio bursts.

1 INTRODUCTION

Fast radio bursts (FRBs) are extragalactic transient radio sources of millisecond duration (Lorimer et al. 2007; Thornton et al. 2013). Some repeat, while most have not been observed to do so (Spitler et al. 2016; Shannon et al. 2018; Kumar et al. 2019; James et al. 2020; The CHIME/FRB Collaboration et al. 2021), and the question of whether or not there are one, two, or more FRB populations remains open. The recent observation of a Galactic magnetar flare with FRB-like properties strongly suggests such objects as an FRB progenitor class (Bochenek et al. 2020; Mereghetti et al. 2020; The Chime/FRB Collaboration et al. 2020). Yet, this flare was three orders of magnitude less powerful than the weakest FRBs, which in turn are orders of magnitude weaker than the most powerful FRBs (Shannon et al. 2018). FRBs may therefore have an unrelated origin.

If the FRB population does originate from young magnetars, they would be expected to be closely correlated with star-forming activities, as observed for two rapid repeaters (Tendulkar et al. 2017; Marcote et al. 2020). However, the single largest sample of localized FRBs comes from the Australian Square Kilometre Array Pathfinder (ASKAP; Bannister et al. 2019; Prochaska et al. 2019b; Bhandari et al. 2020b). The host galaxies of these FRBs – which due to ASKAP's large field of view (FOV) and higher detection threshold tend to be the intrinsically most powerful bursts – do not show evidence for unusual star-forming activity (Bhandari et al. 2020a; Heintz et al. 2020). This allows for the possibility of much of this population to arise from other sources, e.g. compact binary mergers (see Caleb, Spitler & Stappers 2018, and references contained therein).

A useful method to distinguish between these models comes from the evolution of the FRB population on cosmological time-scales. If FRBs originate from young magnetars, they will closely follow the star formation rate (SFR; Metzger, Berger & Margalit 2017), and peak in the redshift range of 1–3. A binary merger scenario however would likely lag the SFR, and possibly result in an FRB rate that is increasing with cosmological time (Cao, Yu & Zhou 2018). As yet, FRB population analysis has not been able to distinguish between these scenarios (Luo et al. 2020; Arcus et al. 2021). Other methods yield mixed results: Hashimoto et al. (2020) find evidence against the redshift evolution of once-off FRBs, and some evidence for redshift evolution of the event rate for repeating FRBs, while Locatelli et al. (2019) find evidence for an evolving FRB population for once-off FRBs. However, neither work follows the comprehensive approach advocated by Connor (2019), by modelling observational biases, and allowing for the confounding effects of the FRB luminosity function.

The FRB luminosity function is interesting in and of itself. Comparisons of the luminosity function of individual repeaters (e.g. Law et al. 2017) to the population as a whole tests the credibility of the one-population model, while evidence for a minimum burst

★ E-mail: clancy.james@curtin.edu.au
† Deceased

energy above that produced by Galactic magnetars would require a separate progenitor class, or at least a separate emission mechanism. Models requiring rare events to explain FRBs can be challenged by measurements of the absolute volumetric rate (Ravi 2019). Estimates of the maximum FRB energy not only challenges theoretical models and pushes up against theoretical limits (Lu & Kumar 2018), but affects the ability to use FRBs as cosmological probes. Estimates of the host contribution to dispersion measure (DM) inform us of the environment surrounding FRB progenitors. Consequently, several groups have begun modelling the FRB population in an attempt to derive these parameters, although the results and methods have been inconsistent (Caleb et al. 2016; Luo et al. 2018, 2020; Lu & Piro 2019; Arcus et al. 2021; Gardenier et al. 2021).

In a companion paper (James et al. 2021a), we present our method to model the FRB population. It uses the methodology advocated by Connor (2019), and first implemented by Luo et al. (2020), while making several significant advances in accuracy and precision, and taking advantage of recent FRB localizations, and fitting for the measured signal-to-noise ratio. This models all known observational biases in detail, allowing us to make accurate and precise estimates of FRB population parameters, and model its cosmological source evolution. Here, we present maximum-likelihood estimates of FRB population parameters using FRBs observed by the Australian Square Kilometre Array Pathfinder (ASKAP) and Parkes, and discuss the implications for the FRB population. Our companion paper also discusses several potential systematic effects in extensive detail,

2 REVIEW OF THE MODEL

In modelling FRB observations, it is critically important to account for a range of observational biases. Our full treatment is contained in a (much lengthier) companion paper, James et al. (2021a). To briefly summarize, we account for telescope beamshape, and reduced observational sensitivity to high-DM, high-width FRBs, as recommended by Connor (2019); and fluctuations in cosmological dispersion measure according to best-fitting cosmological parameters, local contributions from the Milky Way's interstellar medium (ISM) and halo, and a lognormal distribution $p(\mathrm{DM}'_{\mathrm{host}})$ of the host DM contribution, as per Macquart et al. (2020). This latter contribution, defined by

$$p(\mathrm{DM}'_{\mathrm{host}}) = \frac{1}{\mathrm{DM}'_{\mathrm{host}}} \frac{1}{\sigma_{\mathrm{host}}\sqrt{2\pi}} \mathrm{e}^{-\frac{(\log \mathrm{DM}'_{\mathrm{host}} - \mu_{\mathrm{host}})^2}{2\sigma^2_{\mathrm{host}}}}, \quad (1)$$

is fit using the parameters μ_{host} and σ_{host}. The effective host DM, $\mathrm{DM}_{\mathrm{host}}$, corrects the host DM for redshift: $\mathrm{DM}_{\mathrm{host}} = \mathrm{DM}'_{\mathrm{host}}/(1+z)$.

Our model for the FRB population uses a power law with cumulative slope γ and maximum energy E_{max}, such that the probability of observing an FRB above an energy threshold E_{th} is given by

$$p(E > E_{\mathrm{th}}) = \frac{\left(\frac{E_{\mathrm{th}}}{E_{\mathrm{min}}}\right)^{\gamma} - \left(\frac{E_{\mathrm{max}}}{E_{\mathrm{min}}}\right)^{\gamma}}{1 - \left(\frac{E_{\mathrm{max}}}{E_{\mathrm{min}}}\right)^{\gamma}}. \quad (2)$$

The minimum FRB energy is not well constrained by current observations and is set to a very low value of 10^{30} erg. We scale the FRB energy E according to $E \sim \nu^{\alpha}$; for data taken exclusively at L band ($\sim$1.4 GHz), the model is almost degenerate to α (a conclusion also reached by Lu & Piro 2019; Arcus et al. 2021), and so we use a symmetric Gaussian prior of $\alpha = -1.5 \pm 0.3$ (Macquart et al. 2019). We also investigate an alternative interpretation of α, which models the result of Macquart et al. (2019) as a frequency dependent rate, for which the results of Macquart et al. (2019) should be $\alpha = -0.65 \pm 0.3$. We consider both models equally plausible, and treat this uncertainty as a systematic effect. We by-default present results for the spectral index interpretation of α, and show results for the rate interpretation in Appendix A. To cover all results in the literature, we also present results for a uniform prior of $-2.5 \leq \alpha \leq 1$.

We model the evolution of the FRB population $\Phi(z)$ (bursts per proper time per comoving volume) by smoothly scaling the SFR with the parameter n,

$$\Phi(z) = \frac{\Phi_0}{1+z} \left(\frac{\mathrm{SFR}(z)}{\mathrm{SFR}(0)}\right)^n. \quad (3)$$

We take $\mathrm{SFR}(z)$ from Madau & Dickinson (2014),

$$\mathrm{SFR}(z) = 1.0025738(1+z)^{2.7} \left(1 + \left(\frac{1+z}{2.9}\right)^{5.6}\right)^{-1}. \quad (4)$$

We treat E_{max}, γ, α, n, μ_{host}, and σ_{host} as free parameters.

We use a sample of 24 non-localized, and seven localized, FRBs detected by ASKAP, and 20 FRBs detected by the Parkes multibeam system. These have been selected due to them occurring at high Galactic latitudes, where the reduced sensitivity due to high Galactic DM is unimportant. The full telescope beamshape of each of these instruments is modelled in detail in our companion paper, based off the methods of James et al. (2019a), while the reduction in sensitivity to high DMs and widths is modelled using the time- and frequency resolutions of the instruments according to Cordes & McLaughlin (2003).

3 RESULTS

Our single-parameter constraints are given in Fig. 1, showing results with a Gaussian and uniform prior on α. Best-fitting values and confidence limits are calculated using Wilks' theorem (Wilks 1962) (in our companion paper, we construct Bayesian intervals, and find these to be more constraining than those presented here). Tabulated values, and two-parameter plots, are given in the online-only data. We discuss the implications for each parameter individually below.

3.1 Maximum burst energy E_{max}

We find the maximum FRB energy, $\log_{10}E_{\mathrm{max}}$ (erg), to be $41.70^{+0.53}_{-0.06}$ (68 per cent CL). E_{max} is normalized to a bandwidth of 1 GHz at the mean frequency of the data used as inputs (about 1350 MHz), applies to all burst widths, and assumes isotropic emission (no beaming). A strict lower limit on E_{max} is set by the intrinsically brightest localized FRB, 190711, which – using a fluence of 34 Jy ms (Macquart et al. 2020), 1 GHz bandwidth, and $\alpha = -1.5$ – had an energy of $E_{190711} = 10^{41.5}$ erg. For an instrument with a 1 Jy ms threshold, our value of E_{max} leads to a maximum observable redshift of $z = 3.3^{+3}_{-0.2}$.

The preferred value of E_{max} is most strongly correlated with α, which effectively attenuates FRBs as a function of redshift. Upper limits on E_{max} are also strongly correlated with γ, since a large negative value of this parameter makes it unlikely to observe FRBs near E_{max}.

Our value of E_{max} lies in the middle of the values found by other authors. From Fig. A2, fixing $n = 0$ as per Luo et al. (2020) would lead to a less negative value of E_{max}, and greater consistency with that work. The higher values of E_{max} found by Lu & Piro (2019), and used by Arcus et al. (2021), arise in models that assume a 1–1 DM–z relation, which will tend to overestimate E_{max} when an FRB with a significant excess DM – either due to its host or intervening matter – is detected.

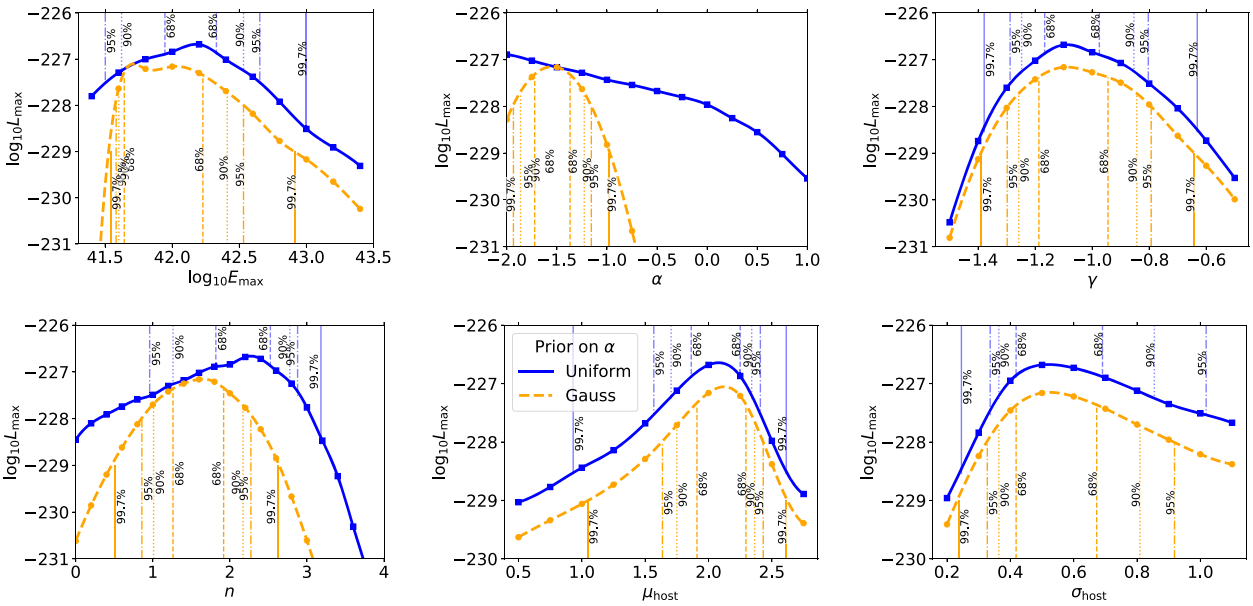

Figure 1. Maximum likelihoods as a function of each considered variable ($E_{\rm max}$, α, γ, n, $\mu_{\rm host}$, $\sigma_{\rm host}$) when marginalized over the other five, both with (orange, lower) and without (blue, upper) a prior on the spectral index α. Calculation results are given by points, with lines drawn using cubic spline smoothing. Vertical lines are single-parameter intervals at the labelled degree of confidence calculated using Wilks' theorem with one degree of freedom. In the case of $\log_{10}E_{\rm max}$, 90 per cent and 95 per cent lower limits are at 41.4.

3.2 Intrinsic luminosity index γ

Our best-fitting power-law index for the FRB population is $-1.09^{+0.14}_{-0.10}$ (68 per cent CL). As discussed by Macquart & Ekers (2018), this parameter primarily governs the degree to which FRBs are viewed from the near or far Universe, with steep values of γ (i.e. below -1.5) leading to observations being dominated by nearby events and the event rate being governed by $E_{\rm min}$. Our result is definitely above this value, which is in agreement with all other calculations. It is however somewhat steeper than the values found by other authors.

Why? Luo et al. (2020) assume no cosmological source evolution, which this parameter is strongly correlated with. An increase in high-redshift FRBs can be due to either a less negative γ, leading to more bursts visible near $E_{\rm max}$ in the larger volume of the distant Universe; or due to an evolving population, as determined by n. This anticorrelation is clearly visible in Fig. A2. Both Arcus et al. (2021) and Lu & Piro (2019) allow source evolution, but assume a 1–1 DM–z relation, implying a large distance for the highest DM FRBs. In order to fit such bursts without overpredicting a large number of lower-energy bursts requires a flat luminosity function.

In the case that all FRBs repeat, with each FRB having the same $E_{\rm max}$ and γ but a distribution of intrinsic rates, the intrinsic luminosity function for the entire population will match that of each FRB. This index has been well measured for FRB 121102, with data giving a range $\gamma_{121102} \approx -0.9 \pm 0.2$ (Law et al. 2017; Gajjar et al. 2018; James 2019). This is consistent with our value for the population. However, should $E_{\rm max}$ vary over FRBs, then the value of γ for the population might be steeper.

Our value of $\gamma < -1$ predicts that $\mathrm{d}N_{\rm FRB}/\mathrm{d}z$ is negative, i.e. it increases in the local (Euclidean) Universe. This is consistent with the recent discovery of very nearby FRBs in the local volume (e.g. Bhardwaj et al. 2021).

3.3 Redshift evolution n

Our best-fitting value of the redshift evolution scaling parameter is $1.67^{+0.25}_{-0.40}$ (68 per cent CL). Under the rate interpretation of α, we find $n = 0.73^{+0.30}_{-0.30}$. In the latter case, $n = 0$ is excluded at only 98 per cent CL. Ignoring Macquart et al. (2019) and taking a uniform prior also disfavours $n = 0$ in the spectral index interpretation (95 per cent CL), but under the rate interpretation, all $0 \leq n \leq 2$ are equally likely.

Our detection of evolution in the FRB population supports conclusions based on FRB localizations, which locate most FRBs within normal host galaxies (Heintz et al. 2020); evidence associating FRBs with magnetars, such as the recent Galactic magnetar outburst (Bochenek et al. 2020; The Chime/FRB Collaboration et al. 2020); and observations of the host environment of FRB 121102 (Michilli et al. 2018), as well as predictions from several classes of progenitor models (Platts et al. 2019).

This does not mean that we have confirmed that FRBs exhibit cosmological evolution identical to the star formation rate however. A more-general model of source evolution, as used by Lu & Piro (2019), simply assumes a $(1+z)^{n'}$ dependence, i.e. it removes the denominator and normalizing constant in equation (4). Near $z = 0$, $n' \equiv 2.7n$ – however, the models will diverge above $z = 1$. A true detection of scaling with the star formation rate would require observations to be consistent with a downturn relative to the $(1+z)^{n'}$ model at and beyond the peak of star forming activity.

Fig. 2 plots the likelihood for both interpretations of α and the $(1+z)^{2.7n}$ model. While the spectral index interpretation of α clearly gives a better fit, the difference in maximum likelihoods between the two source evolution models under the rate assumption is negligible, with the preferred value of n being slightly higher under SFR scaling to compensate for the denominator in equation (4). We therefore cannot claim evidence for a down-turn in the source evolution function due to the peak in the SFR, only that the FRB population is evolving

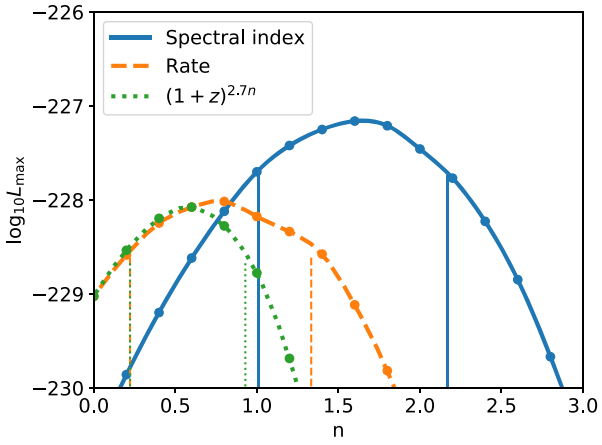

Figure 2. Maximum likelihood fits for source evolution parameter n, for three different cases: interpreting α as a spectral index, and source evolution n scaling the star formation rate as per equation (4) (blue); interpreting α as a frequency dependent rate, again using equation (4) for n-scaling (orange); and with α as a frequency-dependent rate, but n scaling source evolution simply as $(1+z)^{2.7n}$ (green). The vertical lines show 90 CL intervals calculated using Wilks' theorem.

with cosmological time, with the rate per comoving volume greater at higher z.

Our result is still a significant improvement on prior works. Previous calculations have either had to assume a value for FRB source evolution (of $n = 0$ or 1), due to complete degeneracy with α (Lu & Piro 2019), or otherwise could not distinguish between models (Caleb et al. 2016; Lu & Piro 2019; Arcus et al. 2021). As previously noted, and explained in detail in our companion paper, this degeneracy also affects this work. However, the degeneracy is not complete – it is partially broken by the ASKAP/ICS sample of localised FRBs, and by the Parkes sample, which probes to sufficient z to be sensitive to the non-Cartesian nature of the Universe. Of similar works, only Caleb et al. (2016) and Luo et al. (2020) model a telescope beamshape. We show in our companion paper that these authors' assumption of a Gaussian (∼Airy) beamshape for Parkes observations is sufficient, but doing so for ASKAP data – as considered by Luo et al. (2020) – is inappropriate. The inability of Arcus et al. (2021) and Lu & Piro (2019) to exclude $n = 0$ may be due to their lack of beamshape modelling. Including beamshape reveals that a larger fraction of the sky is probed at lower sensitivity, thus increasing sensitivity to FRBs in the local Universe relative to that in the distant Universe. Without this effect, n must be artificially decreased to model the observed number of near-Universe bursts.

3.4 Excess DM distribution

Our model fits a lognormal distribution to $\mathrm{DM_{host}}$, which nominally covers the host galaxy and the immediate FRB environs. The fit will naturally include deviations from the NE2001 DM model of the Milky Way and the assumed halo DM of 50 pc cm^{-3}. We find best-fitting values of $\log_{10}\mu_{\rm host} = 2.11^{+0.18}_{-0.20}$ and $\log_{10}\sigma_{\rm host} = 0.53^{+0.15}_{-0.11}$, with both parameters being relatively independent of the other four. Fig. A2 shows that high values of $\mu_{\rm host}$ and low values of $\sigma_{\rm host}$ are most strongly excluded. The only other authors to fit these parameters are Macquart et al. (2020), who use a sub-set of the data analysed in this work; our fitted value for the mean DM is greater than theirs, but not significantly. Partially, this is because Macquart et al. (2020) do not account for reduced sensitivity to high-DM bursts. Our inclusion of this effect requires a greater intrinsic high-DM population to fit the same observations. Combined with local contributions from the Milky Way's ISM and halo, we estimate a mean non-cosmological DM of $\mathrm{DM_{ISM}} + \mathrm{DM_{halo}} + \mu_{\rm host} = 50 + 35 + 130 = 215$ pc cm^{-3} at $z = 0$. However, this still allows for low values of DM observed by ASKAP (Shannon et al. 2018) and CHIME (CHIME/FRB Collaboration et al. 2019), since both $\mathrm{DM_{host}}$ and the cosmological contribution can vary. This large value of mean non-cosmological contribution helps to explain the observation by Shannon et al. (2018) that the mean DM of the Parkes FRB sample is not as large relative to the ASKAP/ICS sample as would be expected from the relative telescope sensitivities alone.

3.5 The prevalence of FRBs

We estimate the best-fitting absolute rate of FRBs above $E_{\rm min}$, Φ_0, by maximizing the product of p_n between the ASKAP/FE and Parkes/Mb samples with well-constrained $T_{\rm obs}$. We quote Φ_{39}, defined as the estimated rate of bursts above 10^{39} erg (above the maximum allowed value of $E_{\rm min}$ James et al. 2021a) per year at $z = 0$. In the case of our best-fitting model, we find $\Phi_{39} = 8.7^{+1.7}_{-3.9} \cdot 10^4$ bursts Gpc^{-3} yr^{-1} (90 per cent CL), assuming FRBs are unbeamed.

This value is broadly consistent with that estimated by other authors (Lu & Piro 2019; Ravi et al. 2019; Luo et al. 2020), and supports the conclusion that the majority of FRBs must either be repeaters, or cannot be due to known populations of once-off events.

Interestingly, the best-fitting parameter set underpredicts the number of FRBs observed by ASKAP/FE (13.9 versus 20 in 1274.6 d) and overpredicts the number found by Parkes (17.3 versus 12 in 164.4 d). Possible causes of this discrepancy are a minimum FRB energy – or at least a flattening of the distribution at low energies – which would reduce the number of bursts seen by the more-sensitive Parkes telescope; the low number of FRBs detected by Parkes with SNR below 16, as noted by James et al. (2019b), which could be an indicator of a reduced detection efficiency to low-fluence bursts; the observation times reported here being raw observation times, and not accounting for lost effective observation time due to e.g. radio-frequency interference, which is likely more prevalent at Parkes than ASKAP; and simple statistical fluctuations – the product of the ASKAP and Parkes likelihoods will be this or less unlikely 12.4 per cent of the time.

4 CONCLUSION

We have used a precise and accurate method of modelling the results of FRB surveys to fit the measured DM, z, and signal-to-noise ratios of FRBs detected by ASKAP and Parkes. We have carefully selected our data to ensure it is not biased due to under-reporting of observation time, or due to large local DM contributions reducing sensitivity. Crucially, we have included a sample of localized FRBs from ASKAP for which the redshift of the host galaxies is measured.

These modelled observations are tested against a six-parameter model of the FRB population. Using a maximum-likelihood approach, we derive the tightest constraints on FRB population parameters to date. Our value of the maximum FRB energy of $41.70^{+0.53}_{-0.06}$ erg (68 per cent CL) is mid-way between previous estimates. The intrinsic slope of the cumulative luminosity distribution, γ, is found to be $\gamma = -1.09^{+0.14}_{-0.10}$ (68 per cent CL), consistent with, but slightly steeper than, the slope found for FRB 121102. Importantly, we find that the FRB population evolves with redshift, scaling with the star formation rate (SFR) to the power of $1.67^{+0.25}_{-0.40}$ or $0.73^{+0.30}_{-0.30}$, depending on the interpretation of FRB spectral properties. While

we cannot distinguish between SFR-scaling and a model where the FRB population increases as a simple power of $(1+z)^{2.7n}$, in all reasonable scenarios we exclude a non-evolving population at better than 98 per cent CL.

Our best-fitting log-mean host contribution to DM of 130 pc cm^{-3} is also somewhat higher than the standard value of 100 pc cm^{-3}. Such large excess dispersion measures, and a population evolution consistent with star formation, strongly align with the hypothesis of FRBs originating from young magnetars. We caution that these results apply to the total FRB population (which may or may not consist of multiple sub-populations), and only to that part of the population to which the ASKAP and Parkes observations are sensitive.

For a discussion of systematic errors, we refer readers to our companion paper, James et al. (2021a). There, we identify that improved modelling requires better understanding of the spectral behaviour of FRBs and the response of search experiments, and better treatment of the repeating population and luminosity function.

ACKNOWLEDGEMENTS

This research has made use of NASA's Astrophysics Data System Bibliographic Services. This research made use of PYTHON libraries MATPLOTLIB (Hunter 2007), NUMPY (van der Walt, Colbert & Varoquaux 2011), SCIPY (Virtanen et al. 2020), FRB (Prochaska et al. 2019a), and ZDM (James, Prochaska & Ghosh 2021b). This work was performed on the gSTAR national facility at Swinburne University of Technology. gSTAR is funded by Swinburne and the Australian Government's Education Investment Fund. This work was supported by resources provided by the Pawsey Supercomputing Centre with funding from the Australian Government and the Government of Western Australia. This research was partially supported by the Australian Government through the Australian Research Council's Discovery Projects funding scheme (projects DP180100857 and DP210102103).

DATA AVAILABILITY

The data underlying this article will be shared on reasonable request to the corresponding author.

REFERENCES

Arcus W. R., Macquart J.-P., Sammons M. W., James C. W., Ekers R. D., 2021, MNRAS, 501, 5319
Bannister K. W. et al., 2019, Science, 365, 565
Bhandari S. et al., 2020a, ApJ, 895, L37
Bhandari S. et al., 2020b, ApJ, 901, L20
Bhardwaj M. et al., 2021, ApJ, 910, L18
Bochenek C. D., Ravi V., Belov K. V., Hallinan G., Kocz J., Kulkarni S. R., McKenna D. L., 2020, Nature, 587, 59
Caleb M., Flynn C., Bailes M., Barr E. D., Hunstead R. W., Keane E. F., Ravi V., van Straten W., 2016, MNRAS, 458, 708
Caleb M., Spitler L. G., Stappers B. W., 2018, Nature Astron., 2, 839
Cao X.-F., Yu Y.-W., Zhou X., 2018, ApJ, 858, 89
CHIME/FRB Collaboration et al., 2019, Nature, 566, 230
Connor L., 2019, MNRAS, 487, 5753
Cordes J. M., McLaughlin M. A., 2003, ApJ, 596, 1142
Gajjar V. et al., 2018, ApJ, 863, 2
Gardenier D. W., Connor L., van Leeuwen J., Oostrum L. C., Petroff E., 2021, A&A, 647, A30
Hashimoto T. et al., 2020, MNRAS, 498, 3927
Heintz K. E. et al., 2020, ApJ, 903, 152
Hunter J. D., 2007, CSE, 9, 90
James C. W., 2019, MNRAS, 486, 5934
James C. W. et al., 2019a, PASA, 36, e009
James C. W., Ekers R. D., Macquart J.-P., Bannister K. W., Shannon R. M., 2019b, MNRAS, 483, 1342
James C. W. et al., 2020, MNRAS, 495, 2416
James C., Prochaska J., Macquart J.-P., North-Hickey F., Bannister K., Dunning A., 2021a, MNRAS, (Advance Access)
James C. W., Prochaska J. X., Ghosh E. M., 2021b, zdm. Available at: https://zenodo.org/record/5213780#.YRxh5BMzZKA
Kumar P. et al., 2019, ApJ, 887, L30
Law C. J. et al., 2017, ApJ, 850, 76
Locatelli N., Ronchi M., Ghirlanda G., Ghisellini G., 2019, A&A, 625, A109
Lorimer D. R., Bailes M., McLaughlin M. A., Narkevic D. J., Crawford F., 2007, Science, 318, 777
Lu W., Kumar P., 2018, MNRAS, 477, 2470
Lu W., Piro A. L., 2019, ApJ, 883, 40
Luo R., Lee K., Lorimer D. R., Zhang B., 2018, MNRAS, 481, 2320
Luo R., Men Y., Lee K., Wang W., Lorimer D. R., Zhang B., 2020, MNRAS, 494, 665
Macquart J.-P., Ekers R., 2018, MNRAS, 480, 4211
Macquart J.-P., Shannon R. M., Bannister K. W., James C. W., Ekers R. D., Bunton J. D., 2019, ApJ, 872, L19
Macquart J. P. et al., 2020, Nature, 581, 391
Madau P., Dickinson M., 2014, ARA&A, 52, 415
Marcote B. et al., 2020, Nature, 577, 190
Mereghetti S. et al., 2020, ApJ, 898, L29
Metzger B. D., Berger E., Margalit B., 2017, ApJ, 841, 14
Michilli D. et al., 2018, Nature, 553, 182
Platts E., Weltman A., Walters A., Tendulkar S. P., Gordin J. E. B., Kandhai S., 2019, Phys. Rep., 821, 1
Prochaska J. X., Simha S., Law C., Tejos N., Neeleman M., 2019a, FRB. Available at: https://zenodo.org/record/3403651#.YRxkcBMzZKA
Prochaska J. X. et al., 2019b, Science, 366, 231
Ravi V., 2019, Nature Astron., 3, 928
Ravi V. et al., 2019, Nature, 572, 352
Shannon R. M. et al., 2018, Nature, 562, 386
Spitler L. G. et al., 2016, Nature, 531, 202
Tendulkar S. P. et al., 2017, ApJ, 834, L7
The Chime/FRB Collaboration et al., 2020, Nature, 587, 54
The CHIME/FRB Collaboration et al., 2021, preprint (arXiv:2106.04352)
Thornton D. et al., 2013, Science, 341, 53
van der Walt S., Colbert S. C., Varoquaux G., 2011, Comput. Sci. Eng., 13, 22
Virtanen P. et al., 2020, Nature Methods, 17, 261
Wilks S., 1962, Mathematical Statistics. John Wiley and Sons Ltd, New York

SUPPORTING INFORMATION

Supplementary data are available at *MNRASL* online.

Figure S1. Equivalent of Fig. 1, but for the rate interpretation of α: maximum likelihoods as a function of each considered variable ($E_{\rm max}$, α, γ, n, $\mu_{\rm host}$, $\sigma_{\rm host}$) when marginalized over the other five, both with (orange, lower) and without (blue, upper) a prior on the spectral index α.

Figure S2. Two-parameter maximum likelihood results, showing 68 per cent, 90 per cent, and 95 per cent confidence intervals, calculated using Wilks' theorem and a χ^2_2 distribution, for the spectral index interpretation of α, using the Gaussian prior.

Figure S3. Two-parameter maximum likelihood results, showing 68 per cent, 90 per cent, and 95 per cent confidence intervals, calculated using Wilks' theorem and a χ^2_2 distribution, for the spectral index interpretation of α, using the uniform prior.

Figure S4. Equivalent of Fig. A2, but for the rate interpretation of α: two-parameter maximum likelihood results, showing 68 per cent,

90 per cent, and 95 per cent confidence intervals, calculated using Wilks' theorem and a χ^2_2 distribution, using the Gaussian prior.

Figure S5. Equivalent of Fig. A2, but for the rate interpretation of α: two-parameter maximum likelihood results, showing 68 per cent, 90 per cent, and 95 per cent confidence intervals, calculated using Wilks' theorem and a χ^2_2 distribution, using the uniform prior.

Table S1. Confidence limits on single parameters, with a uniform prior (left) and with a Gaussian prior (right) on α, calculated assuming the spectral interpretation of α (see Section 2).

Table S2. Equivalent of Table A1, calculated assuming the rate interpretation of α (see Section 2).

Please note: Oxford University Press is not responsible for the content or functionality of any supporting materials supplied by the authors. Any queries (other than missing material) should be directed to the corresponding author for the article.

This paper has been typeset from a TEX/LATEX file prepared by the author.